



HAL
open science

CoNiMo/Al₂O₃ sulfide catalysts for dibenzothiophene hydrodesulfurization: Effect of the addition of small amounts of nickel

Juan A Medina Cervantes, Rafael Huirache-Acuña, Jorge Noé Díaz de León, Sergio Fuentes-Moyado, Francisco Paraguay-Delgado, Gilles Berhault, Gabriel Alonso-Núñez

► To cite this version:

Juan A Medina Cervantes, Rafael Huirache-Acuña, Jorge Noé Díaz de León, Sergio Fuentes-Moyado, Francisco Paraguay-Delgado, et al.. CoNiMo/Al₂O₃ sulfide catalysts for dibenzothiophene hydrodesulfurization: Effect of the addition of small amounts of nickel. *Microporous and Mesoporous Materials*, 2020, 309, pp.110574. 10.1016/j.micromeso.2020.110574 . hal-03443786

HAL Id: hal-03443786

<https://hal.science/hal-03443786>

Submitted on 23 Nov 2021

HAL is a multi-disciplinary open access archive for the deposit and dissemination of scientific research documents, whether they are published or not. The documents may come from teaching and research institutions in France or abroad, or from public or private research centers.

L'archive ouverte pluridisciplinaire **HAL**, est destinée au dépôt et à la diffusion de documents scientifiques de niveau recherche, publiés ou non, émanant des établissements d'enseignement et de recherche français ou étrangers, des laboratoires publics ou privés.

CoNiMo/Al₂O₃ Sulfide Catalysts for Dibenzothiophene

Hydrodesulfurization: Effect of the Addition of Small Amounts of Nickel

Juan A. Medina Cervantes^a, R. Huirache-Acuña^{a*}, G. Alonso-Núñez^b, J. N. Díaz de León^b,

S. Fuentes Moyado^b, F. Paraguay-Delgado^c, G. Berhault^d

^aFacultad de Ingeniería Química, Universidad Michoacana de San Nicolás de Hidalgo, Ciudad Universitaria, C.P. 58060, Morelia, Michoacán, México.

^bCentro de Nanociencias y Nanotecnología, Universidad Autónoma de México, KM. 107, carretera Tijuana-Ensenada, C.P. 22860, Ensenada, B.C. México.

^cCentro de Investigación en Materiales Avanzados SC. Avenida Miguel de Cervantes Saavedra 120, Complejo Industrial Chihuahua, 31136 Chihuahua, Chih. Mexico

^dInstitut de Recherches sur la Catalyse et l'Environnement de Lyon, CNRS – Université Lyon I, 02 Avenue Albert Einstein, 69100 Villeurbanne, France

Corresponding Autor: Dr. Rafael Huirache-Acuña

Tel.: +52 443 3 273584.

E-Mail: rafael_huirache@yahoo.it

Abstract

Trimetallic CoNiMo hydrodesulfurization (HDS) catalysts were herein synthesized on Al₂O₃ support through an incipient wetness co-impregnation procedure using ammonium heptamolybdate and cobalt (and nickel) acetate as precursors. CoNiMo catalysts were obtained by adding in a small proportion nickel with molar amount representing between 1 and 10 % of the total Co atomic loading. This addition of low amounts of nickel allows keeping the (Co+Ni)/(Co+Ni+Mo) molar ratio close to the optimum value of 0.3. The as-formed catalysts were labeled as CoNi_xMo/Al₂O₃ with x the relative stoichiometry of Ni compared to Co. Catalysts were then characterized by N₂ adsorption-desorption isotherms, X-ray diffraction, ICP-OES spectroscopy, Raman spectroscopy, scanning electron microscopy, high-resolution transmission electron microscopy, and X-ray photoelectron spectroscopy. Catalysts were tested in the HDS of dibenzothiophene (DBT). Results show a significant impact of adding small amounts of nickel to alumina-supported Co-promoted MoS₂ on the final HDS activity. While up to CoNi_{0.03}Mo/Al₂O₃, the resulting HDS activity is hardly influenced by the addition of nickel, a strong beneficial effect is observed for CoNi_{0.05}Mo/Al₂O₃ with an activity reaching a value of $7.2 \times 10^{-7} \text{ mol.g}_{\text{cat}}^{-1}.\text{s}^{-1}$. Increasing further the amount of nickel abruptly decreased the DBT HDS activity. Interpretation of these results is then provided considering the additional role of nickel for improving the intrinsic activity of the HDS sites.

Keywords

Trimetallic catalysts; CoNiMo; hydrodesulfurization; dibenzothiophene.

1. Introduction

In recent years, environmental legislation to improve fuel quality has become more and more strict [1, 2]. The first regulation enforcement was issued in the United States in 1993 to limit the sulfur oxides emission tolerance of transportation vehicles through a reduction from 0.2-0.5 wt % to 500 ppm in sulfur allowed in diesel fuels [3]. Since then, the Environmental Protection Agency (EPA) has decreased twice the maximum sulfur amount authorized in diesel and gasoline. For instance, the current specification of sulfur amount allowed for on-road diesel fuel is 15 ppm [4-5]. This specification has been extended to non-road engine diesel fuels in 2010. This has triggered increasing request for high quality diesel fuels in developed countries. In this respect, in the US market, demand for high quality diesel has increased from 3.16 Mb/d (million barrels per day) in 2005 to 3.31 Mb/d in 2010. Moreover, light cycle oil (LCO) cuts from fluid catalytic cracking (FCC) units are more and more often used in the diesel pool [6]. This higher LCO proportion increases the difficulty for producing clean diesel products since LCO feeds contain a higher amount of highly refractory sulfur compounds such as alkyldibenzothiophenes.

Nowadays, traditional hydrodesulfurization catalysts cannot produce ultra-low sulfur diesel (ULSD) as required by the latest regulations [7] except if using high temperatures and pressure conditions harmful for catalytic life cycle longevity. To improve deep hydrodesulfurization ability, it is necessary to design new catalysts with enhanced desulfurization activity able to efficiently remove sulfur from highly refractory compounds. New more efficient hydrodesulfurization processes can be obtained through the implementation of new HDS technologies [8, 9] or through new catalytic systems using either

new supports [10-17] or new active phases [18-27], the latter approach being the most promising way to enhance the catalytic HDS efficiency [28]. Traditionally, bimetallic HDS catalysts are composed of Mo(W)S₂-based solids supported on Al₂O₃ and promoted by cobalt or nickel. Bimetallic HDS catalysts are susceptible to thermal, chemical or mechanical degradation and/or metal or coke poisoning which often leads to inefficient ways to treat feedstocks [29-31]. To increase the versatility of catalysts to work in various harmful conditions, investigations have tried to develop trimetallic catalysts such as NiMoW, CoNiW, and CoNiMo. In this respect, some studies have been performed considering CoNiMo catalysts for hydrodesulfurization applications [32-41]. However, contradictory results were obtained about the interest of adding a second promoter for increasing HDS activity. While some contributions found that CoNiMo catalysts are less active than traditional bimetallic systems for the HDS of thiophene [37, 38] and of 4,6-DMDBT [41], other studies have reported higher HDS activity for the CoNiMo combination in the HDS of thiophene [39], dibenzothiophene [35, 40], vacuum gas oil [34] or heavy gasoil [33]. However, up to now, a rational interpretation of the positive (or negative) role devoted to the addition of a second promoter to MoS₂-based catalysts has not been proposed yet.

Moreover, the addition of nickel was systematically added in replacement of cobalt in very high amounts with HDS maxima observed at very different Ni/Co atomic ratios (from 0.66 for [34] to 1.54 for [35]). This situation is also worsened by the absence of direct experimental proof showing if separate CoMoS and NiMoS phases are separately formed or if new NiCoMoS sites are created, at least partly.

In this respect, one should also consider the affinity of Ni or Co for the two types of MoS₂ edge sites, the so-called S- and M-edge sites. DFT calculations have indeed demonstrated

that Co and Ni act differently when added as promoter sites of MoS₂ edge planes. Under typical HDS conditions, Co prefers the S-edge and is only present partially on the M-edge resulting in Co coverages of 100 % on the S-edge and 50% on the M-edge. On the opposite, Ni is present on both type of edges with a strong tendency to be incorporated first and only on M-edge sites at low loadings [42-46].

The objective of the present study was therefore to evaluate how the supplementary incorporation of low amounts of nickel in plus of cobalt, on available M-edge sites of MoS₂ slabs as proposed by DFT calculations, can influence the textural, structural and catalytic properties of the resulting CoNiMo catalysts. Nickel promoter atoms have then been added in a small proportion in plus of cobalt atoms to form CoNiMo catalysts with a precise control of the amount and nature of the promoters. The resulting trimetallic catalysts have then been fully characterized before being tested in the HDS of dibenzothiophene in order to determine the exact influence of the addition of low amounts of nickel to Co-promoted MoS₂ on the final HDS catalytic response.

2.Experimental

2.1 Materials

Commercial Al₂O₃ was purchased from Sasol Germany ($S_{\text{BET}} = 200 \text{ m}^2/\text{g}$; $V_{\text{p}} = 0.85 \text{ cm}^3/\text{g}$; average pore diameter: 90 Å). Dibenzothiophene (98 %), decahydronaphthalene (*cis + trans*) (98%), ammonium heptamolybdate tetrahydrate, (NH₄)₆Mo₇O_{24.4} H₂O, cobalt acetate tetrahydrate ($\geq 98\%$) and nickel acetate tetrahydrate (98%) were purchased from Sigma-Aldrich.

2.2 Catalysts Synthesis

Al₂O₃-supported catalysts were prepared using an incipient wetness co-impregnation technique. One bimetallic CoMo catalyst supported on alumina and various Al₂O₃-supported trimetallic CoNiMo catalysts were synthesized. During the catalyst preparation, the (Co)/(Co+Mo) molar ratio was kept constant at 0.3 while small proportions of nickel representing between 1 and 10 % of the cobalt atomic amount were added. Catalysts were labeled as CoNi_xMo/Al₂O₃ with x the theoretical relative stoichiometry of nickel compared to cobalt.

For the bimetallic CoMo/Al₂O₃ catalysts, ammonium heptamolybdate and cobalt acetate tetrahydrate were co-impregnated simultaneously on Al₂O₃ followed by drying under air for 2 h at 393 K in order to reach nominal weight loadings of Mo and Co respectively of 12.0 and 3.0 wt %. After the drying step, the catalysts were calcined for 4 h at 773 K (heating ramp: 2 K/min). The resulting bimetallic oxide catalysts were then sulfided using a H₂/H₂S (15 % vol H₂S) mixture at 673 K for 2 h (20 mL/min; 5 K/min).

For the trimetallic CoNi_xMo/Al₂O₃ catalysts, nickel was added during the preparation in relative atomic percentages (compared to Co) of 1, 3, 5, and 10 at % by adjusting the contents of nickel acetate precursor co-impregnated simultaneously with ammonium heptamolybdate and cobalt acetate onto Al₂O₃. The nominal weight percentage of Mo was kept constant at 12.0 %. After co-impregnation, solids have been dried for 2 h at 393 K before being calcined for 4 h at 773 K (heating ramp: 2 K/min). Finally, oxide solids have been activated under a 15 % vol. H₂S mixture in H₂ for 2 h at 673 K (20 mL/min, 5 K/min) to obtain the trimetallic sulfide catalysts.

2.3 Catalyst Characterization

A Varian Vista-MPX CCD Simultaneous ICP-OES was used to determine the percentages of Co, Ni, and Mo in the sulfided catalysts. An adequate calibration curve with $\pm 10\%$ uncertainty was prepared for each metal involved in the catalysts.

N₂ adsorption-desorption measurements were performed using a Micromeritics GEMINI 2360 equipment. Before analysis, all the samples were degassed under flowing Ar at 423 K for 2 h. Surface areas were calculated using the Brunauer-Emmett-Teller method while the Barrett-Joyner-Halenda (BJH) model was used for pore size determination considering the desorption branch of N₂ isotherms.

X-ray diffraction (XRD) patterns were recorded using a PANalytical X'pert MPD diffractometer equipped with a curved graphite monochromator using the Cu K α radiation ($\lambda = 1.54056 \text{ \AA}$), a Ni filter and an X'Celerator detector. Patterns were acquired in the 5°-80° 2 θ range.

Raman spectra were collected on oxide samples using a Renishaw inVia spectrometer equipped with a Nd:YAG laser ($\lambda = 532 \text{ nm}$). A 1200 lines/mm grating monochromator was used to scatter photons which are then collected on a CCD camera. The spectra resolution was 1 cm⁻¹.

Solids were also analyzed by scanning electron microscopy (SEM) using a JEOL JSM-5300 microscope. Before analysis, samples were deposited on a sample holder with conductive carbon double-sided tape. Samples were observed at 15 \AA and 30 kV. Several regions were

analyzed at different magnifications (500, 2000 and 5000 x) to get a complete surface information.

Transmission electron microscopy (TEM) images were obtained using a JEOL JEM-2200FS (200 kV) microscope in order to get information about MoS₂ slab length and stacking degree. Several zones on the micrographs were observed to perform a statistical analysis of MoS₂ slabs. Samples were ultrasonically dispersed in ethanol before being deposited onto a carbon-coated Cu grid. Average stacking number and average slab lengths were determined as follows:

$$\bar{N} = \frac{\sum_{i=1}^n n_i N_i}{\sum_{i=1}^n n_i}$$

$$\bar{L} = \frac{\sum_{i=1}^n n_i l_i}{\sum_{i=1}^n n_i}$$

With N_i and l_i corresponding respectively to the stacking number and the length of a MoS₂ slab, n_i the number of particles measured in a size range or stacking number of index i .

XPS analyses were performed using a SPECS[®] spectrometer equipped with a PHOIBOS[®] 150 WAL hemispherical energy analyzer with angular resolution lower than 0.5°. The XPS apparatus also possesses a μ -FOCUS 500 X-ray monochromator (Al excitation line). For the sulfide samples, transfer to the XPS chamber was performed under Ar and without contact with air to avoid re-oxidation. Binding energies were referenced to the adventitious C 1s peak (284.8 eV). Background subtraction was performed using a Shirley baseline while mixed Gaussian/Lorentzian functions were used to fit core-level spectra.

2.4 Catalytic Activity

HDS of dibenzothiophene (DBT) was performed using a high-pressure batch Parr reactor with 0.25 g of catalyst. Particle granulometry was selected between 80 and 120 mesh to avoid diffusional limitations. A solution of 2.7 g of DBT in 75 mL of decahydronaphthalene (*cis* + *trans* mixture) was used. The reactor was first heated at 623 K under 690 kPa of H₂ before being purged. This purging procedure was repeated three times. The final pressure was then fixed at 44.8 bars of H₂. Note that HDS conversion and selectivity results are independent of the H₂ pressure above P_{H₂} = 5 bars [47]. Stirring rate was set at 400 rpm to avoid external diffusion limitations. Initial time was fixed when agitation started at the final temperature and pressure conditions. Samples were retrieved every 30 minutes before being analyzed to determine the evolution of the HDS conversion in function of reaction time. The mean standard deviation for catalytic measurements was about 2.5 % [48]. The analysis was performed using an Agilent 7890A gas chromatograph equipped with an HP5 capillary column (30 m length x 0.32 mm internal diameter x 0.25 μm thickness) and an Agilent 355 sulfur chemiluminescence detector (SCD). The reaction products detected by gas chromatography were biphenyl (BP), cyclohexylbenzene (CHB), dicyclohexyl (DCH), and tetrahydrodibenzothiophene (THDBT). The catalytic activity was expressed by the initial reaction rate which was determined from DBT conversion (X_{DBT}) as a function of time (mol_{DBT} transformed per second and per gram of catalyst). The HYD/DDS selectivity ratio was calculated according to HYD and DDS routes products as follows: [(THDBT+CHB+DCH)]/BP.

3. Results and Discussion

3.1. Characterization at the Oxide State

3.1.1. N₂ Physisorption

Figure 1a reports the N₂ adsorption-desorption isotherms of the CoMo/Al₂O₃ reference catalyst and of the CoNi_xMo/Al₂O₃ solids. The isotherms present almost identical type IV profiles characteristic of a mesoporous distribution. Hysteresis loops are well-defined and do not differ from one sample to the next one exhibiting a type H1 shape corresponding either to particles crossed by nearly cylindrical channels or made of aggregates or agglomerates of spheroidal particles [48, 49]. Table 1 reports the textural properties of the CoMo/Al₂O₃ reference and of the various CoNi_xMo/Al₂O₃ solids. BET specific surface areas do not present substantial variations with the increase of the relative Ni atomic content in the CoNiMo catalysts with values ranging between 152 and 176 m²/g. This result shows that modifying the nature of the promoter used (at least in the relative range of this study) does not influence the final textural properties achieved after co-impregnation on the Al₂O₃ support. This is also confirmed by the pore volume values which remain relatively constant around 0.50 cm³/g whatever the relative cobalt and nickel loadings. Figure 1b also reports the BJH pore size distribution observed for all the catalysts. In all cases, identical profiles are obtained showing pore diameter values around 84-87 Å.

3.1.2 X-ray Diffraction

CoMo and CoNi_xMo solids supported on Al₂O₃ were also analyzed by X-ray diffraction at the oxide state after calcination at 773 K for 4 h. All the samples present poorly crystalline structures with only weak diffraction peaks (Figure 2). However, the characterization peaks

of the γ - Al_2O_3 phase can be observed at 2θ values of 32° , 37° , 45° , and 66° corresponding to the (200), (311), (400), and (440) planes respectively [50]. One should also note the absence of any peaks corresponding to segregated Ni or Co oxide phases. All solids also exhibit a distinct diffraction peak at 23.4° corresponding to the MoO_3 phase [51]. Moreover, this peak presents some variations in intensity being the most intense for $\text{CoNi}_{0.01}\text{Mo}/\text{Al}_2\text{O}_3$ before decreasing slightly at higher Ni contents (mainly for $\text{CoNi}_{0.05}\text{Mo}/\text{Al}_2\text{O}_3$ and $\text{CoNi}_{0.1}\text{Mo}/\text{Al}_2\text{O}_3$) suggesting that a small addition of nickel can favor the formation of a more crystalline MoO_3 phase. This point will be further studied by Raman spectroscopy. Another clear diffraction peak can also be noticed at $2\theta = 26.5^\circ$ accompanied by a weaker contribution at $2\theta = 28.4^\circ$. These peaks are generally attributed to the presence of a cobalt molybdate phase, β - CoMoO_4 [52, 53] which is known to reduce the ability to form a cobalt-promoted MoS_2 phase after sulfidation [54-56]. However, the intensity of the cobalt molybdate species does not change whatever the amount of nickel added in plus of cobalt to promote the MoS_2 catalysts suggesting that the cobalt molybdate phase is present in a similar amount and that it should marginally influence the final sulfided state, all other conditions being equal.

3.1.3 Raman Spectroscopy

The various CoNi_xMo catalysts supported on Al_2O_3 were also analyzed by Raman spectroscopy to determine the influence of the addition of nickel on the dispersion and nature of the molybdenum oxide species formed. For comparison purposes, the reference $\text{CoMo}/\text{Al}_2\text{O}_3$ catalyst was also studied. For the Ni-free sample, four main vibration bands

can be observed at 360 cm^{-1} , 820 cm^{-1} , 875 cm^{-1} (weak), and $940\text{-}960\text{ cm}^{-1}$ (Figure 3). The bands at 360 and 820 cm^{-1} were assigned respectively to the deformation and asymmetric stretching modes of MoO_3 species while the bands at 875 and $940\text{-}960\text{ cm}^{-1}$ are due to the asymmetric and symmetric stretching modes of polymolybdate species [33, 57-59].

For $\text{CoNi}_{0.01}\text{Mo}/\text{Al}_2\text{O}_3$, a clear distinguishable new vibration band due to MoO_3 clustering into large polymerized entities appears at 995 cm^{-1} [58, 59] suggesting that the addition of even a small amount of nickel has significant consequences in terms of molybdenum oxide species. This result confirms the preceding observations made by X-ray diffraction. The effect of such a small amount of nickel on the structure of molybdenum oxide species suggest here that this low nickel content probably triggers the condensation of polymolybdate species in such a way that large clusters of MoO_3 are formed after calcination.

This situation however changes when increasing the amount of nickel to 3 % and 5 % suggesting a different role of nickel at these higher Ni contents. Indeed, a progressive disappearance of the signal due to MoO_3 clustered species at 995 cm^{-1} is now observed giving rise only to a shoulder for $\text{CoNi}_{0.03}\text{Mo}/\text{Al}_2\text{O}_3$ and disappearing completely for $\text{CoNi}_{0.05}\text{Mo}/\text{Al}_2\text{O}_3$. This is also accompanied by a shift of the maximum of the main band due to polymolybdate entities from 940 to 960 cm^{-1} when increasing the nickel content from 1 to 3 %. This indicates a progressive higher polymerization degree of the molybdate species from a mixture of MoO_4^{2-} and $\text{Mo}_7\text{O}_{24}^{6-}$ species for $\text{CoNi}_{0.01}\text{Mo}/\text{Al}_2\text{O}_3$ to almost only heptamolybdate entities for $\text{CoNi}_{0.03}\text{Mo}/\text{Al}_2\text{O}_3$ and $\text{CoNi}_{0.05}\text{Mo}/\text{Al}_2\text{O}_3$. Increasing further the Ni content to 10 % leads to a partial loss of defined bands suggesting a higher heterogeneity in terms of molybdate species with a main contribution around 960 cm^{-1} . This latter band

appears also much broader particularly for the higher Raman shift values suggesting the reappearance of some MoO₃ clusters in this case but in a lower proportion.

3.1.4. Scanning Electron Microscopy

Figure 4 reports the SEM images acquired for the CoMo/Al₂O₃ catalyst without Ni and for the CoNi_xMo/Al₂O₃ solids with nickel varying between 1 and 10 wt % of the total initial Co amount. The aspect of all the solids appear similar with a relatively compact shape and the presence in all cases of small grains spread onto the alumina matrix. These results are in agreement with textural properties showing that the addition of small amount of Ni in plus of Co does not influence significantly the porosity and specific surface areas of the alumina-supported Co(Ni)Mo catalysts.

3.2. Characterization at the Sulfide State

3.2.1. Transmission Electron Microscopy

In order to determine how the nature and dispersion of the Mo species at the oxide state may influence the final dispersion of the active phase at the sulfide state, TEM images were acquired for three different cases: 1) the CoMo/Al₂O₃ reference without nickel, 2) the CoNi_{0.05}Mo/Al₂O₃ solid with an intermediate amount of nickel, and 3) the CoNi_{0.1}Mo/Al₂O₃ solid with the highest nickel content (Figure 5). All images show the presence of MoS₂ slabs with characteristic fringes separated by a 0.65 nm interlayer spacing as expected for the 2H-MoS₂ phase [60, 61]. Statistical analysis was then performed in different regions of the solids in order to determine the average slab length and average stacking number of each catalyst. Results are reported in Table 2. The evolution of the average slab length of MoS₂ slabs in

function of the Ni content shows an increase of the slab length from 4.7 nm for CoMo/Al₂O₃ to 4.9 nm for CoNi_{0.05}Mo/Al₂O₃ and 5.4 nm for CoNi_{0.1}Mo/Al₂O₃. The determination of the stacking degree shows similar values for the CoMo/Al₂O₃ and CoNi_{0.05}Mo/Al₂O₃ solids (1.83-1.86) while the sample with the highest Ni content (CoNi_{0.1}Mo/Al₂O₃) presents more stacked slabs (2.23). This shows a progressive but moderate decrease of the dispersion of the MoS₂ slabs as the nickel content increases in the Co(Ni)Mo catalysts with a more marked effect on both average slab length and stacking for the sample with the highest Ni content. This can be compared to our previous Raman results acquired at the oxide state showing a higher propensity of CoNiMo to form MoO₃ clusters. This emphasizes a direct correlation between the ability to disperse molybdenum oxide species and the final dispersion of the MoS₂ slabs.

3.2.2. ICP-OES Analysis

ICP-OES analysis was also performed at the sulfide state to determine the real experimental contents of Ni, Co and Mo. Results are reported in Table 3 for the CoMo/Al₂O₃ reference and for all the CoNi_xMo/Al₂O₃ samples. Mo and Co amounts remain relatively constant for all the samples with values around 3.5-3.8 wt% for Co and 15.8-16.9 wt% for Mo. Note that these values are slightly different to the nominal loading at the oxide state due to the sulfidation procedure. About nickel, experimental values are lower than theoretical ones at very low loadings, slightly for CoNi_{0.01}Mo/Al₂O₃ and more significantly for CoNi_{0.03}Mo/Al₂O₃. However, at higher Ni loadings, the experimental values for the Ni content are very close to the theoretical ones showing some difficulties to incorporate nickel inside cobalt-promoted MoS₂ samples when nickel loadings are very low. However, this

difficulty is relieved at higher nickel contents. In terms of $(\text{Co}+\text{Ni})/(\text{Co}+\text{Ni}+\text{Mo})$ molar ratios, values are relatively constant and close to the 0.3 optimized value for promotion.

3.2.3. X-ray Photoelectron Spectroscopy

X-ray photoelectron spectra have also been acquired for the $\text{CoMo}/\text{Al}_2\text{O}_3$ reference catalyst and for all the Ni-containing alumina-supported CoNi_xMo solids. Note first that due to the low amount of nickel added, this element could not be detected by XPS except for the richest Ni-containing sample ($\text{CoNi}_{0.1}\text{Mo}/\text{Al}_2\text{O}_3$) but still with a too weak signal to allow performing a decomposition procedure into different nickel species. Therefore, only the Mo 3d and Co 2p core level spectra have been analyzed in order to determine the proportion of the different Mo and Co species formed at the sulfide state. Examples of decomposition procedures of Mo 3d and Co 2p core level spectra are provided in Figure 6 about the $\text{CoNi}_{0.05}\text{Mo}/\text{Al}_2\text{O}_3$ catalyst. Mo 3d spectra decomposition procedure has been extensively reported in [62-64]. The Mo 3d core-level spectra region comprises Mo $3d_{5/2}$ and Mo $3d_{3/2}$ contributions. Three Mo 3d doublets can be found: 1) a doublet with binding energies at 229.0 and 232.0 eV corresponding to Mo IV species of the molybdenum sulfide phase, 2) two Mo $3d_{5/2}$ and Mo $3d_{3/2}$ contributions at 230.0 and 233.4 eV due to Mo oxysulfide species with a +V oxidation state and finally 3) a doublet at 232.1 and 235.3 eV corresponding to Mo +VI species of molybdenum oxide. Finally, one should note the presence at lower binding energy values of the S 2s core level contributions. Mo 3d decomposition results are reported in Table 4. In the case of $\text{CoNi}_{0.01}\text{Mo}/\text{Al}_2\text{O}_3$, adding Ni leads to a marked increase in the proportion of molybdenum oxysulfide species from 8.3 % for $\text{CoMo}/\text{Al}_2\text{O}_3$ to 30.2 % for $\text{CoNi}_{0.01}\text{Mo}/\text{Al}_2\text{O}_3$ while the MoS_2 phase proportion decreases significantly to 64.7 % from

82.5% for CoMo/Al₂O₃. Increasing further the Ni content confirms a progressive higher difficulty to sulfide the molybdenum species. Indeed, for CoNi_{0.03}Mo/Al₂O₃, instead of an increased proportion of partially-sulfided Mo oxysulfides, a higher proportion of completely non-sulfided Mo oxide species can be noticed (15.9 % vs 5.1 % for CoNi_{0.01}Mo/Al₂O₃). However, increasing further the nickel content like for CoNi_{0.05}Mo/Al₂O₃ and CoNi_{0.1}Mo/Al₂O₃ does not modify significantly anymore the proportion of Mo oxide species. One should also note that this increase in Mo oxide species occurs at the expense of Mo oxysulfide species decreasing once again to low percentages between 5.9 % and 8.0 %. Finally, the proportion of completely sulfided Mo species goes back progressively to values close to the one observed for the Ni-free CoMo/Al₂O₃ catalyst. In this respect, the proportions in MoS₂ phase for CoNi_{0.05}Mo/Al₂O₃ and CoNi_{0.1}Mo/Al₂O₃ are 81.2 and 79.3 % respectively, close to 82.5 % for CoMo/Al₂O₃.

Results about the Co 2p decomposition core level spectra are also reported in Table 4. The Co 2p_{3/2} core level spectrum also comprises three different contributions with their respective satellites [65-67] corresponding to CoO_x oxide species, the promoted CoMoS phase and the non-promoted CoS_x sulfide species. CoO_x, CoMoS, and CoS_x species give rise to Co 2p_{3/2} contributions at binding energies respectively around 782 eV, 778.3-778.9 eV, and 777.6-777.9 eV [68, 69]. Results show that the CoNi_xMo samples are slightly better sulfided than the CoMo/Al₂O₃ reference except for the richest Ni-containing CoNi_{0.1}Mo/Al₂O₃ catalyst. Moreover, for nickel contents up to the CoNi_{0.05}Mo/Al₂O₃ case, the proportion of promoted CoMoS phase does not change significantly remaining between 64 and 69 %. The only exception is the CoNi_{0.1}Mo/Al₂O₃ system which presents significant increases in CoO_x and

non-promoted CoS_x species, respectively to 16.2 and 27.0 % while the lowest percentage of promoted phase was also found for this sample (56.8 %).

The Mo 3d and Co 2p XPS results correlate nicely with Raman results at the oxide state. Indeed, for $\text{CoNi}_{0.01}\text{Mo}/\text{Al}_2\text{O}_3$, the appearance of a significant MoO_3 contribution leads to a higher difficulty to sulfidation with the lowest percentage of MoS_2 phase and a higher proportion of incompletely sulfided Mo oxysulfides. Increasing the nickel content like for $\text{CoNi}_{0.03}\text{Mo}/\text{Al}_2\text{O}_3$ and $\text{CoNi}_{0.05}\text{Mo}/\text{Al}_2\text{O}_3$ leads back progressively to better completely sulfided MoS_2 species while the percentage of promoted phase does not change in agreement with the progressive disappearance of agglomerated MoO_3 clusters at the oxide state. Finally, the reappearance of MoO_3 clusters for the $\text{CoNi}_{0.1}\text{Mo}/\text{Al}_2\text{O}_3$ case induces this time a lower formation of the Co-promoted phase suggesting in this latter case that a too high addition of nickel would lead to a competition between Ni and Co for accommodating MoS_2 edge planes.

3.3. HDS Catalytic Activity Evaluation

The evolution of the initial reaction rate for the hydrodesulfurization of dibenzothiophene in function of the Ni content show a marked and contrasted evolution of the HDS activity with the amount of nickel present (Table 5). For $\text{CoNi}_{0.01}\text{Mo}/\text{Al}_2\text{O}_3$, the activity tends to decrease slightly to $5.9 \times 10^{-7} \text{ mol}_{\text{DBT}} \cdot \text{g}_{\text{cat}}^{-1} \cdot \text{s}^{-1}$ from $6.3 \times 10^{-7} \text{ mol}_{\text{DBT}} \cdot \text{g}_{\text{cat}}^{-1} \cdot \text{s}^{-1}$ for the $\text{CoMo}/\text{Al}_2\text{O}_3$ reference. This limited decrease can be ascribed to the lower sulfidation degree of the molybdenum species as shown by XPS. This moderate loss of activity cannot be retrieved when increasing the Ni content like for $\text{CoNi}_{0.03}\text{Mo}/\text{Al}_2\text{O}_3$. This can be due probably to a still too high proportion of MoO_x species (Table 4) confirming the difficulty to sulfide the MoO_3 clusters observed at the oxide state (Figure 3). On the opposite, increasing further the nickel

amount to 5 % (CoNi_{0.05}Mo/Al₂O₃) leads to a net increase of the HDS activity to 7.2×10^{-7} mol_{DBT}.g_{cat}⁻¹.s⁻¹. This reflects the optimized preparation achieved in this case without significant MoO₃ clustering (Figure 3) and with a high proportion of MoS₂ species (81.2 %). This is also accompanied by the maintaining of the promoted CoMoS phase to a proportion similar to the nickel-free CoMo/Al₂O₃ reference. Markedly, the CoNi_{0.1}Mo/Al₂O₃ sample with the richest Ni content shows the lowest HDS activity, much lower even than the CoMo/Al₂O₃ reference (3.8×10^{-7} mol_{DBT}.g_{cat}⁻¹.s⁻¹). This is directly related here to the lowest proportion of promoted phase as determined by XPS for this sample (56.8 %).

The hydrodesulfurization of dibenzothiophene also occurs through two parallel pathways: 1) the direct desulfurization route (DDS) leading to direct C-S bond rupture and formation of biphenyl and 2) the so-called hydrogenating route (HYD) in which hydrogenation of one of the two aromatic rings occurs before C-S hydrogenolysis leading to cyclohexylbenzene. Table 5 reports the HYD/DDS ratio observed for each catalyst. Results show similar HYD/DDS ratios in all cases with the noticeable exception of CoNi_{0.05}Mo/Al₂O₃ with a HYD/DDS ratio of 0.39. This indicates that in this particular case the promoted active sites are more hydrogenating in character suggesting that the successful incorporation of nickel into Co-doped MoS₂ slabs as observed in this case can modify partly the selectivity properties without decreasing both the degree of sulfidation and the amount of CoMoS phase.

The HDS results should also be analyzed taking into account the fact that the MoS₂ dispersion also varies when increasing the nickel content. In this respect, the determination of turnover frequency (TOF) values allow evaluating the relative intrinsic activities of the previous catalysts and the enhancement of the catalytic efficiency resulting from the incorporation of nickel into cobalt-promoted MoS₂ catalysts independently of the dispersion parameter. TOF

values are determined considering a geometrical model for MoS₂ slabs [59] in which the total number of Mo atoms in the slabs and the number of Mo edge atoms (considered as the only active HDS sites) are obtained as follows:

$$\text{Mo}_t = 3n^2 + 3n + 1$$

$$\text{Mo}_e = 6n$$

$$\text{With } n(\text{\AA}) = \frac{L}{2 \times 3.2} \text{ (L = slab length, and } d_{\text{Mo-Mo}} = 3.2 \text{ \AA}).$$

Slab lengths are determined by TEM statistical analysis while the number of MoS₂ edge sites can be calculated considering the Mo loading as determined by ICP-OES and the MoS₂ proportion obtained by XPS. TOF values are then obtained as follows:

$$\text{TOF}(\text{h}^{-1}) = r \cdot N / n_{(\text{MoS}_2\text{e})}$$

with *r*, the DBT activity at 623 K, *N* the Avogadro number and *n*_(MoS₂e) the number of Mo edge atoms as MoS₂.

Results are herein determined for three cases: the CoMo/Al₂O₃ reference, the most active catalyst, CoNi_{0.05}Mo/Al₂O₃, and finally the richest Ni containing CoNi_{0.1}Mo/Al₂O₃. Going from the CoMo/Al₂O₃ reference to CoNi_{0.05}Mo/Al₂O₃, TOF values increase from 7.0 h⁻¹ to 7.9 h⁻¹ showing an enhancement by ~15 % of the intrinsic activity resulting from an optimized incorporation of Ni into a cobalt-promoted Al₂O₃ catalyst. This underlines clearly that the controlled incorporation of even quite low amounts of nickel increases the intrinsic activity of HDS catalysts.

In this respect, when comparing CoNi_{0.05}Mo/Al₂O₃ to the CoMo/Al₂O₃ reference, the enhanced activity cannot be attributed neither to a higher dispersion of the active phase (cf. Table 2) nor to a higher sulfidation degree or proportion of CoMoS phase (cf. Table 4).

Therefore, and since the Co content is similar in both cases, the HDS enhancement should only result from the incorporation of Ni onto the M-edge sites of MoS₂ slabs since not occupied by cobalt and creating therefore new NiMoS sites, as suggested by various DFT studies [42-46]. A rough approximation can then be made about the intrinsic activity of such NiMoS sites considering that all the Ni atoms are incorporated onto the MoS₂ edge sites. The resulting increased HDS activity compared to CoMo/Al₂O₃ would indicate that these new NiMoS sites are about 60 % more active than the CoMoS sites. Note however that these CoMoS sites are not expected to present similar intrinsic activities since comprising a majority of sites on the S-edge planes but also a minority on the M-edge sites. This should lead to different intrinsic activities for these CoMoS sites depending on their location on the edge planes. Anyway, this result, even if approximate, confirms that the additional incorporation of Ni atoms on M-edge sites in plus of Co promoters results in the formation of highly active promoted active sites.

Increasing further the nickel content to about 10 % like for CoNi_{0.1}Mo/Al₂O₃ leads to a strong decrease of the TOF value to 4.7 h⁻¹. This low intrinsic activity results mainly from a significant decrease of the proportion of CoMoS phase as observed by XPS (Table 4). This would suggest that at higher Ni loading, nickel has a stronger affinity for the M-edge sites of MoS₂ slabs [45, 46]. Nickel then starts competing with cobalt for the occupation of the M-edge planes. This results in a loss of CoMoS phase. This also suggests that the Co-promoted sites present on the M-edge planes are intrinsically more active than the more numerous CoMoS entities present on the S-edge planes since otherwise no decrease in activity would have been observed. This result is in agreement with previous DFT observations showing that the maximum HDS activity is reached when an optimum amount of Co is present on the

M-edge sites pointing to the superior activity of CoMoS sites when formed on M-edge planes [46, 60]. This was also confirmed recently by Ding et al. [70] through DFT calculations. Indeed, the C-S hydrogenolysis ability of the Co-promotion on M-edge planes was found intrinsically more efficient than on S-edge sites.

4. Conclusion

In the present study, the influence of incorporating low amounts of nickel into cobalt-promoted MoS₂ catalysts was herein evaluated. Nickel was incorporated in relative proportions of 1, 3, 5 or 10 atomic percentages of the cobalt initially present. The resulting catalysts were characterized at both the oxide and sulfide states showing that optimum conditions of preparation were reached when about 5 % of nickel was added in plus of cobalt. Before and after this optimum, substantial MoO₃ clustering is observed at the oxide state leading either to difficulties for sulfiding the molybdenum species at very low Ni loadings or to a lower formation of the promoted phase if nickel is added in excess. HDS optimum efficiency is therefore reached for the CoNi_{0.05}Mo/Al₂O₃ catalyst. Determination of TOF values allows to ascertain the beneficial effect resulting from an optimized incorporation of nickel into cobalt-promoted MoS₂ slabs showing that the controlled preparation of alumina-supported trimetallic CoNiMo catalysts is a promising way to enhance the HDS catalytic performance of MoS₂-based solids through addition of nickel onto partly available M-edge planes

Acknowledgments

We appreciate the support of: SENER-PEMEX through the project 117373, CONACYT project 182191 and CIC-UMSNH 2020. We also appreciate the technical support provided by F. Ruiz, M. Estrada, D. Dominguez, J.A. Díaz, I. Gradilla, E. Aparicio at CNyN-UNAM Mexico. Thanks to E. Guerrero L and W. Antunez for their technical help at NaNoTech – CIMAV Mexico.

References

- [1] G. Berhault G, Metal sulfides: novel synthesis methods and recent developments, in: *New Materials for Catalytic Applications* (V.I. Parvulescu, E. Kemnitz, Eds), Elsevier, Amsterdam, 2016, pp. 313-360. <https://doi.org/10.1016/B978-0-444-63587-7.00010-X>.
- [2] B. Guichard, M. Roy-Auberger, E. Devers, B. Rebours, A.A. Quoineaud, M. Digne, *Appl. Catal. A*. 367 (2009) 1-8. <https://doi.org/10.1016/j.apcata.2009.07.024>.
- [3] C. Song, X. Ma, *Appl. Catal. B* 41 (2003) 207-238. [https://doi.org/10.1016/S0926-3373\(02\)00212-6](https://doi.org/10.1016/S0926-3373(02)00212-6).
- [4] K.H. Choi, Y. Sano, Y. Korai, I. Mochida, *Appl. Catal. B* 49 (2004) 219-225. <https://doi.org/10.1016/j.apcatb.2003.12.007>.
- [5] H. Farag, I. Mochida, *J. Colloid. Interface Sci.* 372 (2012) 121-129. <https://doi.org/10.1016/j.jcis.2012.01.019>.
- [6] Z. Liu, Y. Zheng, W. Wang, Q. Zhang, L. Jia, *Appl. Catal. A* 339 (2008) 209-220. <https://doi.org/10.1016/j.apcata.2008.01.018>.
- [7] A. Stanislaus, A. Marafi, M.S. Rana, *Catal. Today* 153 (2010) 1-68. <https://doi.org/10.1016/j.cattod.2010.05.011>.

- [8] S.V. Budukva, P.M. Eletsii, O.O. Zaikina, G.A. Sosnin, V.A. Yakovlev. Secondary Middle Distillates and Their Processing (Review). *Petroleum Chemistry* 2019; 59(9):941-955. <https://doi.org/10.1134/S0965544119090044>.
- [9] I.V. Babich, J.A. Moulijn, *Fuel* 82 (2003) 607-631. [https://doi.org/10.1016/S0016-2361\(02\)00324-1](https://doi.org/10.1016/S0016-2361(02)00324-1).
- [10] A. Guevara-Lara, R. Bacaud, M. Vrinat, *Appl. Catal. A* 328 (2007) 99–108. <https://doi.org/10.1016/j.apcata.2007.05.028>.
- [11] Y. Li, D. Pan, C. Yu, Y. Fan, X. Bao, *J. Catal.* 286 (2012) 124–136. <https://doi.org/10.1016/j.jcat.2011.10.023>.
- [12] F. Rashidi, T. Sasaki, A.M. Rashidi, A.N. Kharat, K.J. Jozani, *J. Catal.* 299 (2013) 321–335. <https://doi.org/10.1016/j.jcat.2012.11.012>.
- [13] W. Chen, F. Maugé, J. Van Gestel, H. Nie, D. Li, X. Long, *J. Catal.* 304 (2013) 47–62. <https://doi.org/10.1016/j.jcat.2013.03.004>.
- [14] M. Sun, D. Nicosia, R. Prins, *Catal. Today* 86 (2003) 173–189. [https://doi.org/10.1016/S0920-5861\(03\)00410-3](https://doi.org/10.1016/S0920-5861(03)00410-3).
- [15] A. López-Benítez, G. Berhault, A. Guevara-Lara, *J. Catal.* 344 (2016) 59–76. <https://doi.org/10.1016/j.jcat.2016.08.015>.
- [16] A. López-Benítez, G. Berhault, L. Burel, A. Guevara-Lara, *J. Catal.* 354 (2017) 197-212. <https://doi.org/10.1016/j.jcat.2017.08.027>.
- [17] R. Huirache-Acuña, E.M. Rivera-Muñoz, B. Pawelec, M. Ostrooumov, R. Maya-Yescas, J.L. Rico, *Catal. Today* 220-222 (2014) 301-309. <https://doi.org/10.1016/j.cattod.2013.07.019>.

- [18] Z. Vit, D. Gulkova, L. Kaluza, S. Bakardieva, M. Boaro, *Appl. Catal. B* 100 (2010) 463–471. <https://doi.org/10.1016/j.apcatb.2010.08.022>.
- [19] J.A. Schaidle, N.M. Schweitzer, O.T. Ajenifujah, L.T. Thompson, *J. Catal.* 289 (2012) 210–217. <https://doi.org/10.1016/j.jcat.2012.02.012>.
- [20] J.A. Cecilia, A. Infantes-Molina, E. Rodríguez-Castellón, A. Jiménez-López, *J. Catal.* 263 (2009) 4–15. <https://doi.org/10.1016/j.jcat.2009.02.013>.
- [21] Y.K. Lee, S.T. Oyama, *J. Catal.* 239 (2006) 376–389. <https://doi.org/10.1016/j.jcat.2005.12.029>.
- [22] A.W. Burns, A.F. Gaudette, M.E. Bussell, *J. Catal.* 260 (2008) 262–269. <https://doi.org/10.1016/j.jcat.2008.10.001>.
- [23] S.T. Oyama, Y.K. Lee, *J. Catal.* 258 (2008) 393–400. <https://doi.org/10.1016/j.jcat.2008.06.023>.
- [24] G. Berhault, P. Afanasiev, H. Loboué, C. Geantet, T. Cseri, C. Pichon, C. Guillot-Deudon, A. Lafond, *Inorg. Chem.* 48 (2009) 2985–2992. <https://doi.org/10.1021/ic802074k>.
- [25] S.T. Oyama, H. Zhao, H.J. Freund, K. Asakura, R. Włodarczyk, M. Sierka, *J. Catal.* 285 (2012) 1–5. <https://doi.org/10.1016/j.jcat.2011.08.006>.
- [26] A.I. D’Aquino, S.J. Danforth, T.R. Clinkingbeard, B. Ilic, L. Pullan, M.A. Reynolds, B.D. Murray, M.E. Bussell, *J. Catal.* 335 (2016) 204–214. <https://doi.org/10.1016/j.jcat.2015.12.006>.
- [27] H. Zhao, S.T. Oyama, H.J. Freund, R. Włodarczyk, M. Sierka, *Appl. Catal. B* 164 (2015) 204–216. <https://doi.org/10.1016/j.apcatb.2014.09.010>.
- [28] F. Liu, S. Xu, L. Cao, Y. Chi, T. Zhang, D. Xue, *J. Phys. Chem. C* 111 (2007) 7396–7402. <https://doi.org/10.1021/jp068482+>.

- [29] I. Chorkendorff and J.W. Niemantsverdriet, *Concepts of Modern Catalysis and Kinetics*, Wiley-VCH Verlag GmbH & Co. KGaA, 2005, p. 1-21.
- [30] M. Hussain, J.S. Yun, S.K. Ihm, N. Russo, F. Geobaldo, *Ind. Eng. Chem. Res.* 50 (2011) 2530-2535. <https://doi.org/10.1021/ie100574w>.
- [31] M.E. Pacheco, V.M. Martins Salim, J.C. Pino, *Ind. Eng. Chem. Res.* 50 2011 5975-5981. <https://doi.org/10.1021/ie1023595>.
- [32] D.K. Lee, I.C. Lee, S.I. Woo, *Appl. Catal. A* 109 (1994) 195-210. [https://doi.org/10.1016/0926-860X\(94\)80118-5](https://doi.org/10.1016/0926-860X(94)80118-5).
- [33] S. Badoga, A. Ganesan, A.K. Dalai, S. Chand, *Catal. Today* 291 (2017) 160-171. <https://doi.org/10.1016/j.cattod.2017.01.005>.
- [34] O.V. Klimov, K.A. Nadeina, P.P. Dik, G.I. Koryakina, V.Yu. Pereyma, M.O. Kazakov, S.V. Budukva, E.Yu. Gerasimov, I.P. Prosvirin, D.I. Kochubey, A.S. Noskov, *Catal. Today* 271 (2016) 56-63. <https://doi.org/10.1016/j.cattod.2015.11.004>.
- [35] A.V. Mozhaev, P.A. Nikulshin, A.I.A. Pimerzin, K.I. Maslakov, A.A. Pimerzin, *Catal. Today* 271 (2016) 80-90. <https://doi.org/10.1016/j.cattod.2015.11.002>.
- [36] C.L. Yin, H. Liu, X.H. Li, Y.P. Wang, B. Liu, L.Y. Zhao, C.G. Liu, *Catal. Lett.* 144 (2014) 285-292. <https://doi.org/10.1007/s10562-013-1131-2>.
- [37] F. Severino, J. Laine, A. López-Agudo, *J. Catal.* 189 (2000) 244-246. <https://doi.org/10.1006/jcat.1999.2683>.
- [38] J. Laine, J.L. Brito, F. Severino, *J. Catal.* 131 (1991) 385-393. [https://doi.org/10.1016/0021-9517\(91\)90273-7](https://doi.org/10.1016/0021-9517(91)90273-7).
- [39] C. Cáceres, J.L.G. Fierro, A. López Agudo, F. Severino, J. Laine, *J. Catal.* 97 (1986) 219-227. [https://doi.org/10.1016/0021-9517\(86\)90052-7](https://doi.org/10.1016/0021-9517(86)90052-7).

- [40] W. Qian, Y. Hachiya, D. Wang, K. Hirabayashi, A. Ishihara, T. Kabe, H. Okazaki, M. Adachi, *Appl. Catal. A* 227 (2002) 19-28. [https://doi.org/10.1016/S0926-860X\(01\)00919-X](https://doi.org/10.1016/S0926-860X(01)00919-X).
- [41] R. Sadeghbeigi. *Fluid Catalytic Cracking Handbook*, 2nd Ed. Gulf Professional Publishing, Houston, 2000, p.84.
- [42] H. Schweiger, P. Raybaud, H. Toulhoat, *J. Catal.* 212 (2002) 33-38. <https://doi.org/10.1006/jcat.2002.3737>.
- [43] M. Sun, A.E. Nelson, J. Adjaye, *J. Catal.* 226 (2004) 32-40. <https://doi.org/10.1016/j.jcat.2004.05.005>.
- [44] M. Sun, A.E. Nelson, J. Adjaye, *J. Catal.* 226 (2004) 41-53. <https://doi.org/10.1016/j.jcat.2004.04.023>.
- [45] E. Krebs, B. Silvi, P. Raybaud, *Catal. Today* 130 (2008) 160-169. <https://doi.org/10.1016/j.cattod.2007.06.081>.
- [46] K. Marchand, C. Legens, D. Guillaume, P. Raybaud, *Oil & Gas Sci tech – Rev. IFP* 64 (2009) 719-730. <https://doi.org/10.2516/ogst/2009037>.
- [47] S. Texier, G. Berhault, G. Pérot, F. Diehl, *Appl. Catal. A* 293 (2005) 105-119. <https://doi.org/10.1016/j.apcata.2005.07.026>
- [48] G. Alonso, G. Berhault, A. Aguilar, V. Collins, C. Ornelas, S. Fuentes, R.R. Chianelli, *J. Catal.* 208 (2002) 359-369. <https://doi.org/10.1006/jcat.2002.3553>.
- [49] G. Leofanti, M. Padovan, G. Tozzola, B. Venturelli, *Catal. Today* 41 (1998) 207–219. [https://doi.org/10.1016/S0920-5861\(98\)00050-9](https://doi.org/10.1016/S0920-5861(98)00050-9).
- [50] S. Badoga, R.V. Sharma, A.K. Dalai, J. Adyaje, *Appl. Catal. A* 489 (2015) 86-97. <https://doi.org/10.1016/j.apcata.2014.10.008>.

- [51] S. Badoga, K. Chandra Mouli, K.K. Soni, A.K. Dalai, J. Adyaje, *Appl. Catal. B* 125 (2012) 67-84. <https://doi.org/10.1016/j.apcatb.2012.05.015>.
- [52] N-Q. Bui, C. Geantet, G. J. Catal. 330 (2015) 374-386. <https://doi.org/10.1016/j.jcat.2015.07.031>.
- [53] N-Q. Bui, C. Geantet, G. Berhault, *Appl. Catal. A* 572 (2019) 185-196. <https://doi.org/10.1016/j.apcata.2019.01.006>.
- [54] K. Inamura, K. Uchikawa, S. Matsuda, Y. Akai, *Appl. Surf. Sci.* 121-122 (1997) 468-475. [https://doi.org/10.1016/S0169-4332\(97\)00331-0](https://doi.org/10.1016/S0169-4332(97)00331-0).
- [55] L. Peña, D. Valencia, T. Klimova, *Appl. Catal. B* 147 (2014) 879-887. <https://doi.org/10.1016/j.apcatb.2013.10.019>.
- [56] Y. Saih, K. Segawa, *Appl. Catal. A* 353 (2009) 258-265. <https://doi.org/10.1016/j.apcata.2008.10.037>.
- [57] A.N. Desikan, L. Huang, S.T. Oyama, *J. Phys. Chem.* 95 (1991) 10050-10056. <https://doi.org/10.1021/j100177a080>.
- [58] X. Carrier, J.F. Lambert, M. Che, *J. Am. Chem. Soc.* 119 (1997) 10137-10146. <https://doi.org/10.1021/ja971981r>.
- [59] A. López-Benítez, G. Berhault, A. Guevara-Lara, *Appl. Catal. B* 213 (2017) 28-41. <https://doi.org/10.1016/j.apcatb.2017.04.058>.
- [60] M. Ramos, G. Berhault, D.A. Ferrer, B. Torres, R.R. Chianelli, *Catal. Sci. Tech.* 2 (2012) 164-178. <https://doi.org/10.1039/C1CY00126D>.
- [61] M. Perez De la Rosa, S. Texier, G. Berhault, A. Camacho, M.J. Yácaman, A. Mehta, S. Fuentes, J.A. Montoya, F. Murrieta, R.R. Chianelli, *J. Catal.* 225 (2004) 288-299. <https://doi.org/10.1016/j.jcat.2004.03.039>.

- [62] T. Weber, J.C. Muijsers, J.H.M.C. Van Wolput, C.P.J. Verhagen, J.W. Niemantsverdriet, *J. Phys. Chem.* 100 (1996) 14144–14150. <https://doi.org/10.1021/jp961204y>.
- [63] J. Lu, P. Qi, Y. Peng, Z. Meng, Z. Yang, W. Yu, Y. Qian, *Chem. Mater* 13 (2001) 2169–2172. <https://doi.org/10.1021/cm010049j>.
- [64] Y. Sakashita, *Surf. Sci.* 489 (2001) 45–58. [https://doi.org/10.1016/S0039-6028\(01\)01127-X](https://doi.org/10.1016/S0039-6028(01)01127-X).
- [65] A. Galtayries, S. Wisniewski, J. Grimblot, *J. Electron Spectros Related Phenomena* 87 (1997) 31–44. [https://doi.org/10.1016/S0368-2048\(97\)00071-6](https://doi.org/10.1016/S0368-2048(97)00071-6).
- [66] A.M. Venezia, *Catal. Today* 77 (2003) 359–370. [https://doi.org/10.1016/S0920-5861\(02\)00380-2](https://doi.org/10.1016/S0920-5861(02)00380-2).
- [67] J.C. Dupin, D. Gonbeau, I. Martin-Litas, P.h. Vinatier, A. Levasseur, *Appl. Surf. Sci.* 173 (2001) 140–150. [https://doi.org/10.1016/S0169-4332\(00\)00893-X](https://doi.org/10.1016/S0169-4332(00)00893-X).
- [68] A.D. Gandubert, E. Krebs, C. Legens, D. Costa, D. Guillaume, P. Raybaud, *Catal. Today* 130 (2008) 149–159. <https://doi.org/10.1016/j.cattod.2007.06.041>.
- [69] D.G. Castner, P.R. Watson, *J. Phys. Chem.* 95 (1991) 6617–6623. <https://doi.org/10.1021/j100170a044>.
- [70] S.J. Ding, S.J. Jiang, Y.S. Zhou, Q. Wei, W.W. Zhou, *J. Catal.* 345 (2017) 24–38. <https://doi.org/10.1016/j.jcat.2016.11.011>.

Table 1. BET specific surface area, total pore volume and pore diameter of the trimetallic CoNi_xMo/Al₂O₃ catalysts. Comparison to the CoMo/Al₂O₃ reference.

Al₂O₃- Supported Sample	Specific surface area (m².g⁻¹)	Total pore volume (cm³.g⁻¹)	Pore diameter (nm)
CoMo	157	0.46	8.52
CoNi _{0.01} Mo	162	0.49	8.54
CoNi _{0.03} Mo	176	0.52	8.35
CoNi _{0.05} Mo	170	0.50	8.38
CoNi _{0.1} Mo	152	0.46	8.66

Table 2. TEM statistical determination of the MoS₂ slab dispersion (average slab length and average stacking number) for CoMo/Al₂O₃, CoNi_{0.05}Mo/Al₂O₃ and CoNi_{0.1}Mo/Al₂O₃.

Al₂O₃-	Average	Average
Supported	Slab Length	Stacking
Sample	(nm)	Number
CoMo	4.7	1.83
CoNi _{0.05} Mo	4.9	1.86
CoNi _{0.1} Mo	5.4	2.23

Table 3. ICP-OES analysis of the Ni, Co, and Mo contents and determination of the (Co+Ni)/(Co+Ni+Mo) molar ratio. Values in parentheses are theoretical Ni contents.

Al₂O₃- Supported Sample	% Mo (wt %)	% Co (wt %)	% Ni (wt %)	(Co+Ni)/(Co+Ni+Mo) Molar Ratio
CoMo	15.8	3.6	/	0.27
CoNi _{0.01} Mo	16.0	3.5	0.02 (0.03)	0.26
CoNi _{0.03} Mo	16.4	3.8	0.03 (0.09)	0.28
CoNi _{0.05} Mo	16.9	3.6	0.13 (0.15)	0.27
CoNi _{0.1} Mo	16.8	3.6	0.30 (0.31)	0.28

Table 4. Respective proportions of the different Mo and Co species obtained from the decomposition of Mo 3d and Ni 2p XPS core level spectra.

Al₂O₃- Supported Sample	CoO_x (%)	CoMoS (%)	CoS_x (%)	MoO_x (%)	MoO_xS_y (%)	MoS₂ (%)
CoMo	13.9	68.7	17.3	9.1	8.3	82.5
CoNi _{0.01} Mo	8.3	66.9	24.7	5.1	30.2	64.7
CoNi _{0.03} Mo	10.8	63.8	25.4	15.9	8.0	76.1
CoNi _{0.05} Mo	8.9	68.6	22.5	12.9	5.9	81.2
CoNi _{0.1} Mo	16.2	56.8	27.0	13.6	7.1	79.3

Table 5. Initial reaction rate and HYD/DDS ratio in the HDS of dibenzothiophene for the trimetallic CoNi_xMo/Al₂O₃ catalysts. Comparison to the CoMo/Al₂O₃ reference (T = 623 K, P_{H2} = 44.8 bars, 0.25 g catalyst, 2.7 g DBT/75 mL decahydronaphthalene).

Al₂O₃- Supported Sample	Initial Reaction Rate (10⁻⁸ mol_{DBT}·g_{cat}⁻¹·s⁻¹)	HYD/DDS ratio
CoMo	63	0.249
CoNi _{0.01} Mo	59	0.264
CoNi _{0.03} Mo	56	0.248
CoNi _{0.05} Mo	72	0.390
CoNi _{0.1} Mo	38	0.263

Figure captions.

Figure 1. A) N₂ adsorption-desorption isotherms and B) BJH pore size distribution of the supported trimetallic CoNi_xMo/Al₂O₃ catalysts. Comparison to the CoMo/Al₂O₃ reference.

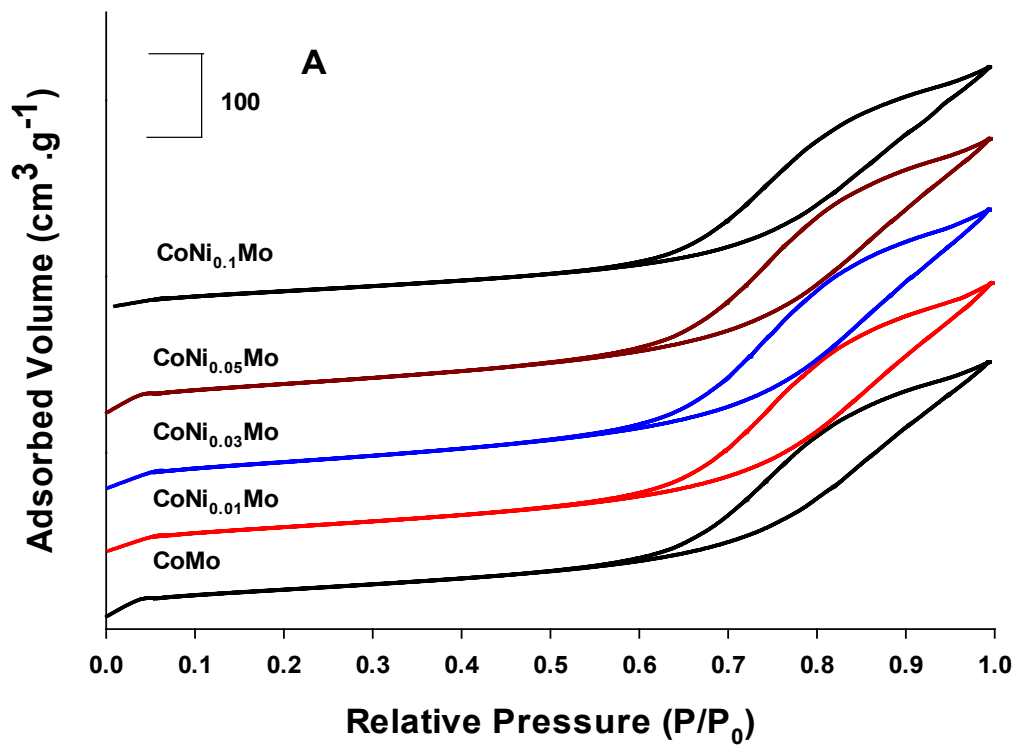
Figure 2. XRD patterns for supported trimetallic CoNi_xMo/Al₂O₃ catalysts. Comparison to the CoMo/Al₂O₃ reference.

Figure 3. Raman spectra of supported trimetallic CoNi_xMo/Al₂O₃ catalysts. Comparison to the CoMo/Al₂O₃ reference.

Figure 4. SEM images of the alumina-supported catalysts: A) CoMo, B) CoNi_{0.01}Mo, C) CoNi_{0.03}Mo, D) CoNi_{0.05}Mo, E) CoNi_{0.1}Mo.

Figure 5. TEM images of the alumina-supported a) CoMo, b) CoNi_{0.05}Mo, and c) CoNi_{0.1}Mo catalysts.

Figure 6. Examples of XPS decomposition of Mo 3d and Co 2p core emission line regions for the CoNi_{0.05}Mo sulfided catalyst.



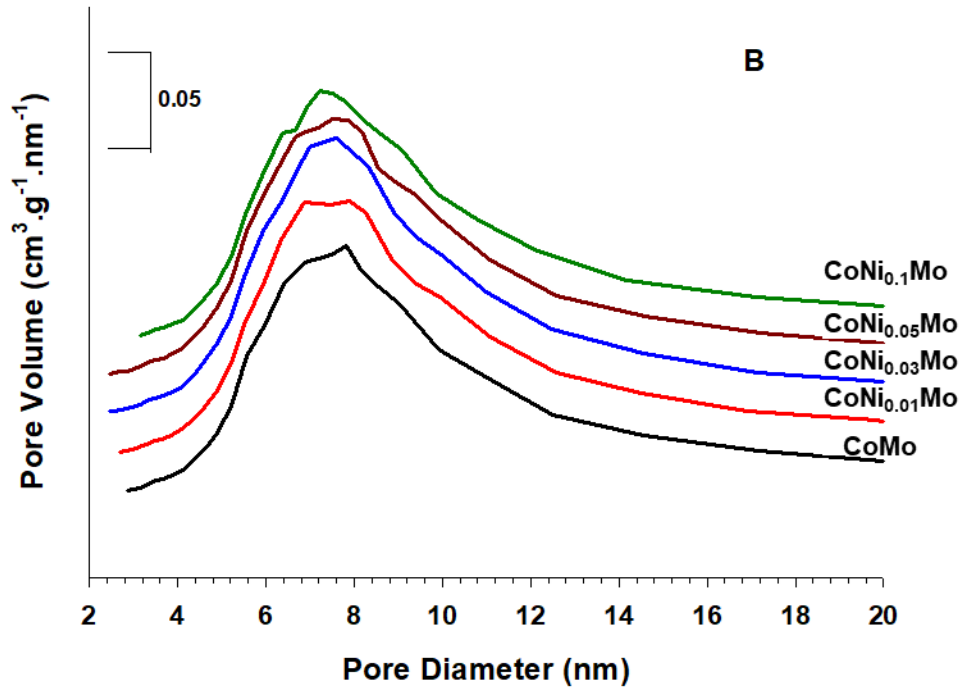


Figure 1.

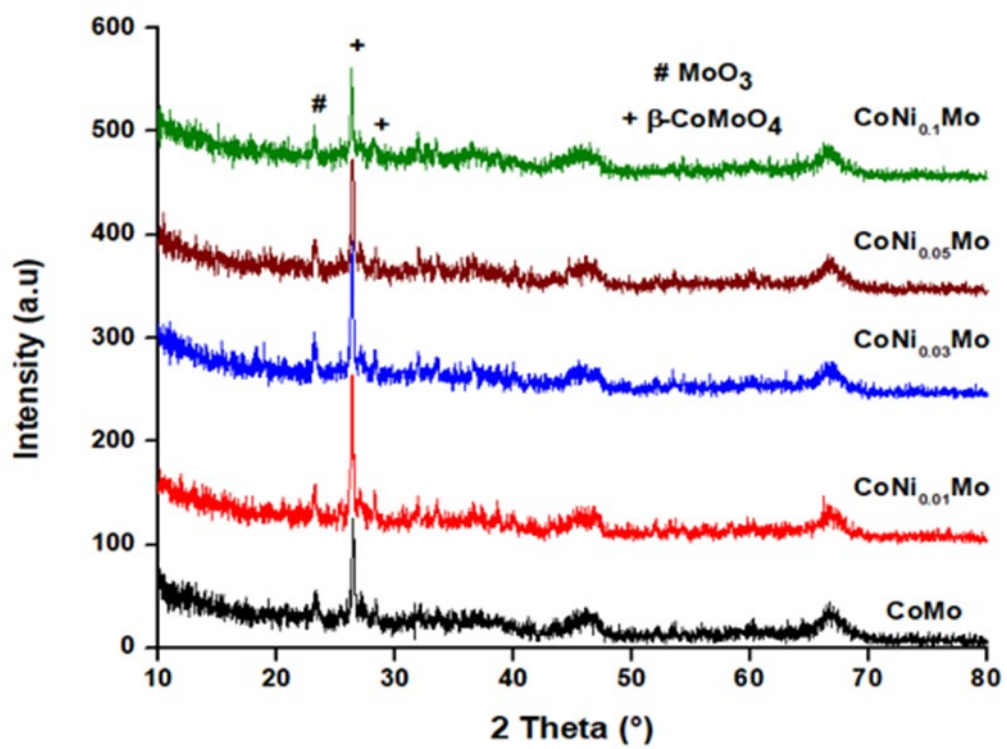


Figure 2.

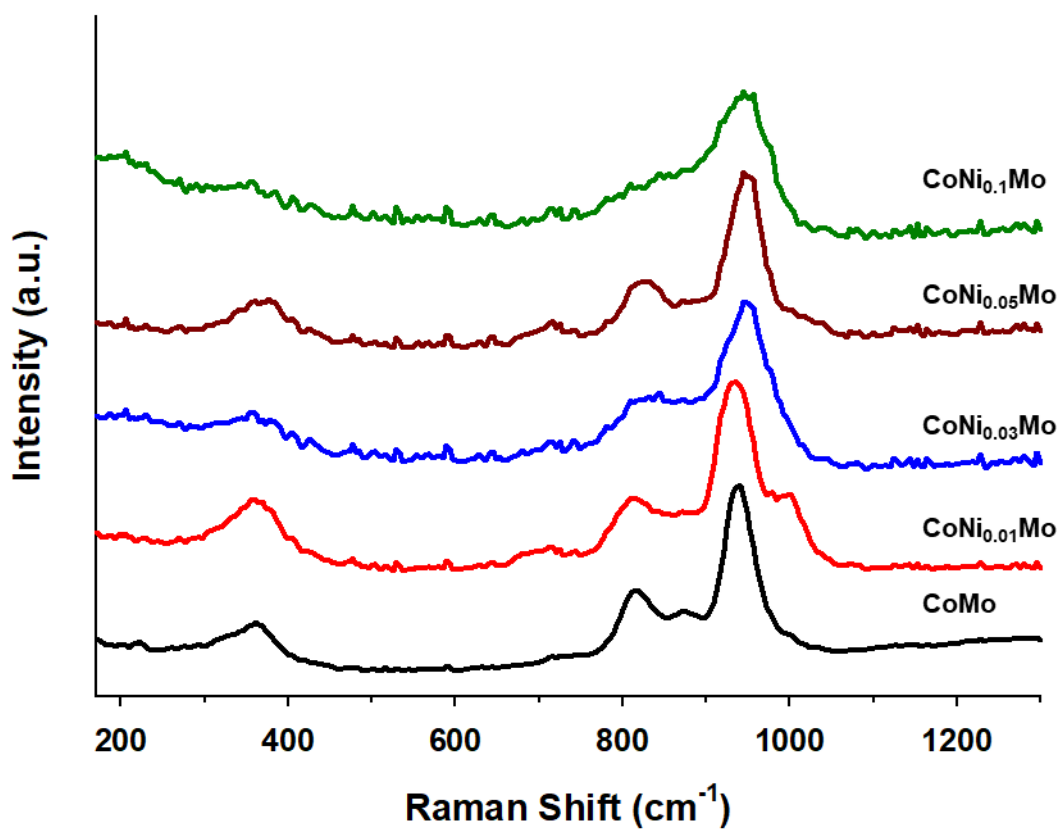


Figure 3.

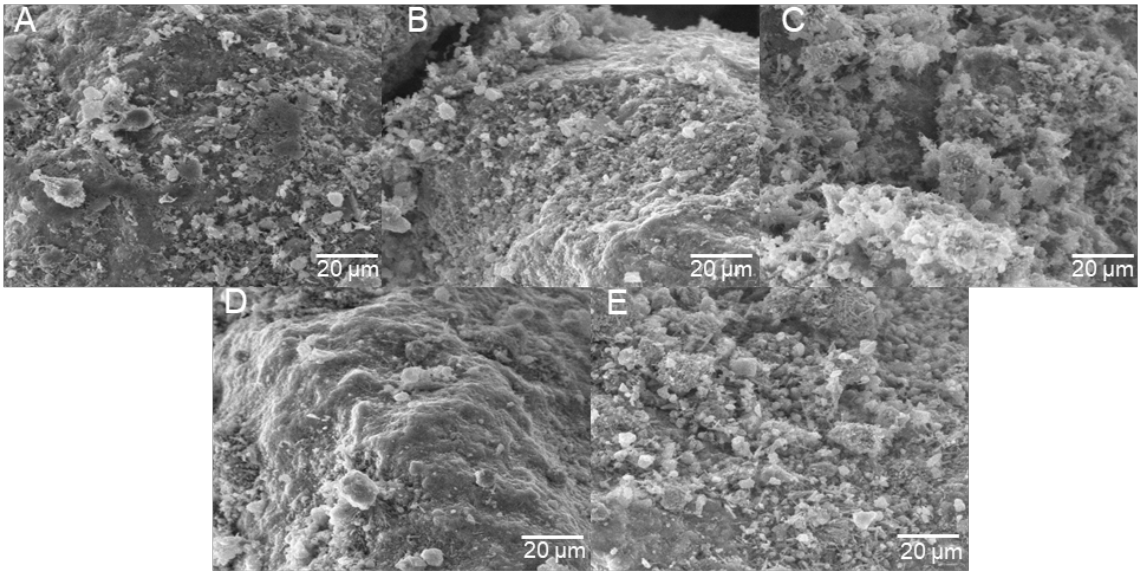


Figure 4.

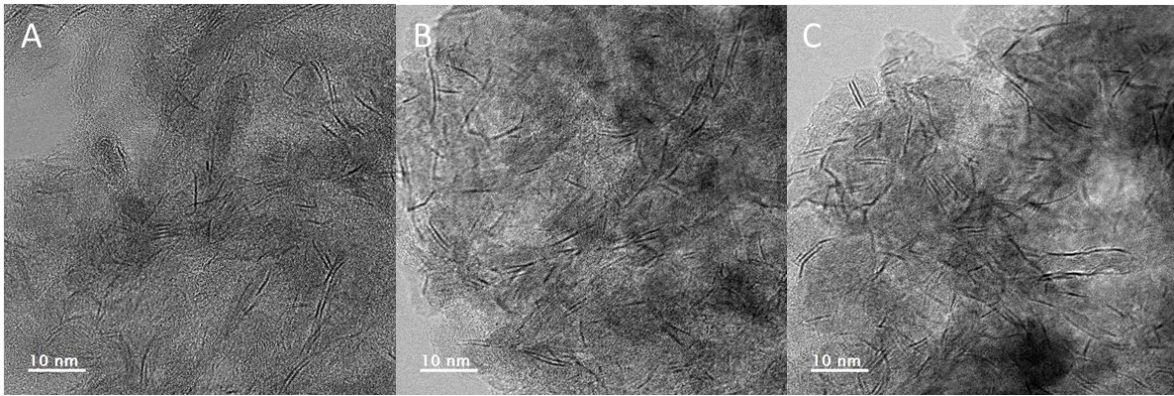


Figure 5.

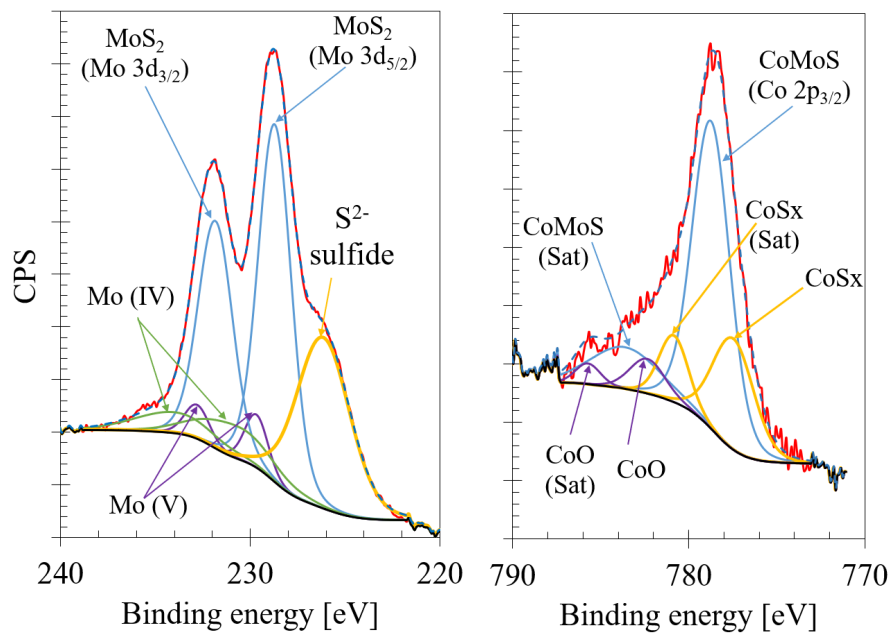


Figure 6